Journal of Sustainability for Energy
https://www.acadlore.com/journals/JSE

Prediction and Assessment of Solar Radiation Intensity Shade Projection in Jayapura City, Indonesia: Optimisation of Solar Energy Utilisation

Usman Tahir[1], Gatot Ciptadi[2], Marjono[3], Abdul Wahid Hasyim[4], Sudirman Syam[5*]

[1] Department of Electrical Engineering, Faculty of Industrial and Earth Technology, Universitas Sains dan Teknologi Jayapura, 99351 Jayapura, Indonesia
[2] Department of Animal Science, Faculty of Animal Husbandry, Brawijaya University, 65145 Malang, Indonesia
[3] Department of Mathematics, Faculty of Mathematics and Natural Sciences, Brawijaya University, 65145 Malang, Indonesia
[4] Department of Urban and Regional Planning, Faculty of Engineering, Brawijaya University, 65145 Malang, Indonesia
[5] Department of Electrical Engineering, Faculty of Science and Technology, Nusa Cendana University, 85228 Kupang, Indonesia

* Correspondence: Sudirman Syam (sudirman_s@staf.undana.ac.id)

Received: 07-15-2024 **Revised:** 08-16-2024 **Accepted:** 08-28-2024

Citation: U. Tahir, G. Ciptadi, Marjono, A. W. Hasyim, and S. Syam, "Prediction and assessment of solar radiation intensity shade projection in Jayapura City, Indonesia: Optimisation of solar energy utilisation," *J. Sustain. Energy*, vol. 3, no. 3, pp. 171–186, 2024. https://doi.org/10.56578/jse030303.

Abstract: Jayapura City, Indonesia, presents significant potential for solar energy utilisation, driven by its high solar radiation levels. However, the presence of urban obstacles, such as buildings, trees, and varied topography, can obstruct the direct transmission of solar radiation to the ground, thereby reducing its efficiency for solar energy systems. This study aims to develop a methodology for predicting and assessing the shade projection of solar radiation intensity across Jayapura City. A quantitative descriptive approach was employed, involving the measurement of elevation and azimuth angles using Global Positioning System (GPS) technology. Data were analysed using RETScreen and Sun Locator Pro (SLP) software. The analysis of the collected data facilitated the generation of a detailed shade projection map, which can be utilised to optimise the placement of solar panels and enhance the performance of the city's Solar Power Generation System (SPGS). The findings indicated that the highest elevation angle occurred at 12:00 pm in March. In September, the sun's position was nearly directly above the equator, leading to a minimal shadow ratio (SR = 0.08), with the projection closely aligned with the object. The azimuth angle, measured at noon, exhibited an extreme angular shift, reflecting the standard reference towards the north (180° at noon). This study demonstrates the potential of this methodology to inform the strategic placement of solar infrastructure, improving the efficiency and efficacy of solar power systems in urban environments characterised by complex topographies.

Keywords: Solar radiation; Shade projection; Azimuth angle; Elevation angle; Solar energy optimisation; Solar power generation system (SPGS); Jayapura City; Solar panel placement

1 Introduction

Solar energy has become a global spotlight as a clean and sustainable alternative energy source [1, 2]. As an abundant renewable energy source, solar energy has great potential to be developed in Indonesia, especially in areas with high solar radiation intensity, such as Jayapura City in Papua Province. Papua is the largest province of Indonesia, located in the central part of Papua Island, or the easternmost part of Indonesia, bordering the country of Papua New Guinea. Papua Province, with its capital Jayapura as the 33rd province in the territory of the Republic of Indonesia (RI) in the eastern part, has its uniqueness with various flora and fauna and even natural conditions that are still natural. The climate in Papua Province is classified as tropical, with rainfall varying in each region. Land use is around 100,000 ha from 410,660 km^2, and slopes and cliffs dominate the land surface [3]. In addition, Jayapura has solar radiation intensity. However, unique geographical conditions, such as mountains and frequent cloud cover,

cause significant fluctuations in solar radiation intensity. According to the Jayapura City profile, its area is located at $1°28'17.26'' - 3°58'0.82''$S and $137°34'10.6'' - 141°0'8.22''$E, where the topography varies greatly, ranging from plains, slopes, and hills with an altitude of around 700 meters above sea level [4]. The average solar radiation in Indonesia is 4 to 5.7 $\mathrm{kWh/m^2}$, with Papua and West Nusa Tenggara (NTB) among the provinces with radiation of more than 5 $\mathrm{kWh/m^2}$. According to data from the Directorate General of New Renewable Energy and Energy Conservation in the 2016 EBTKE statistics, Papua Province has a solar power potential of 2,035 MW. Compared to the installed capacity of power plants of only 86.67 MW, the potential for solar power is the primary alternative for electricity supply in Papua.

Indonesia, which has abundant availability of solar energy the day and the year, has a positive impact on the implementation of solar power [5–7]. Data from the Ministry of Energy and Mineral Resources of the RI in 2023 shows that the potential for solar energy development in the RI reaches approximately 3,300 GW, and the potential for rooftop PV is approximately 32.5 GW. In this regard, optimal solar energy utilisation requires a deep understanding of the solar radiation conditions at the location. The existence of various factors that affect the intensity of solar radiation, such as weather conditions, time, and the presence of obstacles, is a challenge in the planning and construction of PLTS. Height can affect the clarity of shadows based on the principles of physics and geometry [8]. The contour of the land and other objects can affect how shadows are formed and seen in mountainous areas. Shadows will appear when an object blocks light from a source. In other words, when an obstructing object is between the light source and the surface, a shadow will be formed on the opposite side of the object. If there is an obstructing object, such as a building or tree, the resulting shadow can be longer and last longer, especially when the sun is in a low position (morning or evening). Obstructing objects can increase the duration of the shadow because the sunlight is blocked for longer before reaching the surface [9].

On the other hand, the output power of photovoltaic (PV) modules depends on the solar radiation conditions and cell temperature. When the PV system is under uniform irradiation conditions, the electricity generated by each module is the same, so the overall output power is the sum of the individual module powers. On the other hand, the radiation is not uniform if the system is partially shaded, which causes power loss. Partial shading can be caused by dirt and surrounding elements such as vegetation (trees) and buildings. Other conditions affect PV system performance, such as wind, tilt angle, and dust, which can also sometimes cause partial shading [10–15]. Several methodologies and shadow effect estimation have been proposed regarding shadow prediction, such as SOMBRERO [16] and SHADING [17]. According to the study by Sinapis et al. [18], a result model was developed that considers shadow effects. Regarding shadow prediction, an accurate representation of the installation and the barrier elements was done in SketchUp. A Python script was developed to calculate the shadow table for each specific factor, such as azimuth and solar elevation angles. The PV cell was modelled with a simplified double-diode model. Then Melo et al. [19] proposed a methodology to calculate the shadow fraction and irradiance in a three-dimensional model and developed a plug-in for sketchup to test the methodology.

Furthermore, exposure to sunlight and the sustainability of renewable energy technology require the utilization of solar energy potential [20–22]. Globally, only one percent of solar radiation is utilized from the world's current energy consumption. Then, the output characteristics of solar power harvesting collectors are highly dependent on temperature and nonlinear radiation. The nature of solar panel modules does not match the PV array, even in slightly shaded conditions, preventing the module from receiving the same amount of sunlight throughout the day [23]. The trigger for the mismatch in the electrical characteristics of solar panels, which reduces the PV output energy [24] and the size and type of PV array configuration [25], is the shadow pattern as a form of shadow. Due to variations in land contours and the presence of surrounding objects, this condition will be worse if the entire shadow occurs for an extended period. Thus, fluctuations in solar radiation intensity due to weather factors and atmospheric conditions are often obstacles in planning and optimizing the use of solar panels. Therefore, this study aims to develop an accurate methodology for predicting and measuring the projection of solar radiation intensity shade in Jayapura City as a model for other cities in Indonesia with similar geographical conditions. The results of this study are expected to provide significant contributions to spatial planning, location selection, and optimal solar energy system design to increase the use of solar energy in Indonesia.

2 Methodology

2.1 Study Areas

Geographically, Papua Province is at the coordinate point: Latitude $1°28'17.26'' - 3°58'0.82''$S and Longitude $137°34'10.6'' - 141°0.8'22''$E. Meanwhile, Jayapura City is correct at the geographical coordinate point, $2°32'$S and $140°43'$E. The city has a unique and strategic geographical condition with an area of $940\ \mathrm{km^2}$ divided into five districts: South Jayapura, North Jayapura, Muara Tami, Abepura, and Heram District. The boundaries of Jayapura City are in the north with the Pacific Ocean, in the east with Wutung, Sandaun Province, Papua New Guinea, in the south with Keerom Regency, and in the west with Jayapura Regency. Figure 1 shows the USTJ - Organda housing in Hedam Village as the research location. This housing is adjacent to the USTJ housing located south

of the Organda housing. While the Cyclop mountain fault, there are Emerauw hills to the east and west of the housing with an elevation of $70 - 730$ m. Based on observations from Google Earth, the USTJ housing is located at $2°36''12''$SL, $140°39'26''$EL, elevation 16.21 m , and the Organda housing is at $2°35''48''$SL, $140°39'34''$EL, elevation 18.86 m.

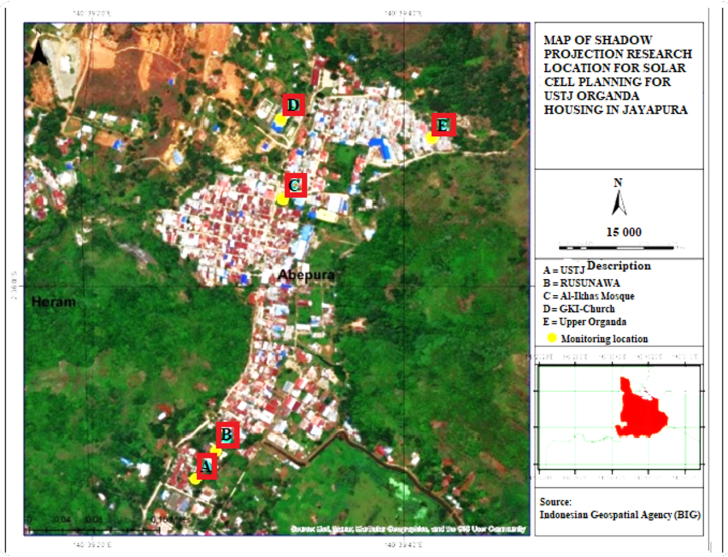

Figure 1. USTJ – Organda housing research location area

Figure 2. GPS – Garmin Etrex 22x

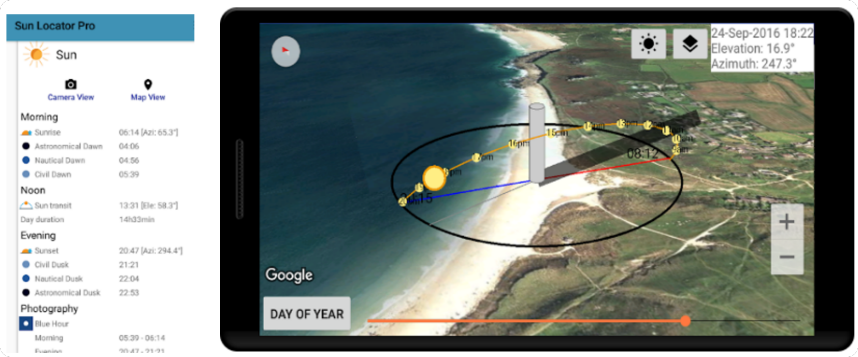

Figure 3. SLP

2.2 Research Procedure

2.2.1 Determination of geographic coordinates

Primary data in the form of determining geographic coordinates is obtained from direct measurement results using a measuring instrument in the form of a Garmin eTres 22x GPS to determine the geographic coordinate point

site (Figure 2). The Garmin eTrex 22x GPS is a portable navigation device for outdoor activities such as hiking, cycling, and other adventures. This device's primary function is to accurately determine geographic position and provide the necessary navigation information. This tool has two main functions. The first is as a navigation tool for determining position, creating routes, and navigation. The second function is to create a mapping in the form of topoActive maps and reference points.

2.2.2 Determining the sun's elevation angle

The sun's elevation angle is determined using the SLP application, as shown in Figure 3. The SLP application can support the acquisition of elevation angle and azimuth measurement results for the sun's position so that it can easily describe the percentage of shadow length and direction projection (tilt value) of sunlight at any time from an object that blocks sunlight at a geographic coordinate point.

Figure 4. Solar Power Meter (SPM – SM 206)

The SLP app is a digital tool designed to help users understand and predict the sun's position at a given location and time. The app can display highly accurate information about the sun's path, sunrise and sunset times, and moon phases using GPS technology and a digital compass. The app accurately predicts the sun's location at a given time and year. That includes sunrise and sunset times, golden hour, and blue hour. Sun Locator can also show the path of the sun throughout the day. This information is beneficial for planning outdoor activities that require optimal sunlight. In addition, some Sun Locator apps also provide features to track moon phases, allowing users to view the sun's position in real-time through the phone's camera using augmented reality technology.

2.2.3 Measurement of solar radiation intensity

This is an essential parameter in the study of climatology, meteorology, and renewable energy as a form of solar energy utilization. The intensity of solar radiation is also commonly termed irradiance, which refers to the amount of solar radiation received by a surface per unit area and per unit time. The results of radiation intensity measurements are often expressed in W/m^2 and can vary depending on the time of measurement and weather conditions. Factors that affect solar intensity are:

1) Atmospheric conditions: Clouds, pollution, and humidity can affect how much radiation reaches the Earth's surface.

2) Position of the Sun: The angle and position of the Sun in the sky throughout the day and year affect the intensity of radiation received.

3) Distance of the Earth from the Sun: The distance of the Earth to the Sun varies throughout the year due to the Earth's elliptical orbit, which also affects the intensity of radiation.

This study measured solar radiation intensity measurements throughout the day when the sun was bright in certain months. There are four groups of solar radiation intensity measurements, including the beginning of the rainy season (MH-1), the end of the rainy season (MH-2), the beginning of the dry season (MK-1), and the end of the dry season (MK-2). Figure 4 shows the Solar Power Meter (SPM-SM206) used in this measurement. At the same time, the Restscreen software obtained real-time data, such as air temperature, humidity, solar radiation intensity, earth temperature, and atmospheric pressure.

2.3 Data Processing

Figure 5 shows a concept diagram of data processing to determine shadow projection with the following stages:

- Pre-processing: Satellite data and the SL Pro application are processed to produce data ready for analysis, such as vegetation index, surface height, and slope gradient.

- Solar radiation modeling: A solar radiation model based on tropical climate conditions estimates the intensity of solar radiation at each point on the earth's surface.

- Shade projection analysis: A shade projection analysis is carried out at each point using SL Pro application data and information on the location and height of buildings and vegetation.

- Regression analysis: Using the linear regression method, a pair of coordinate points (latitude and longitude) and the slope of a line (azimuth angle) can be determined, and then the projection of incoming rays in the form of a straight line on a horizontal surface can be described as a shadow projection pattern.

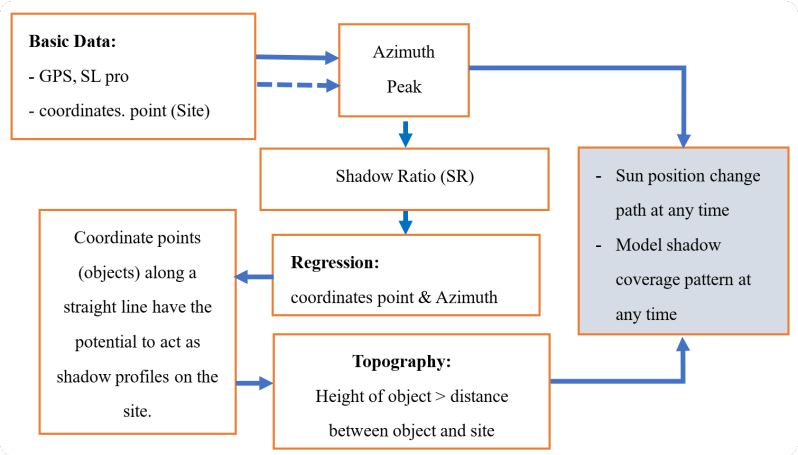

Figure 5. Concept diagram of shade coverage

2.4 Data Analysis

2.4.1 Determining the sun's angular position

In this paper, using quantitative methods and deductive approaches, the sun's angular position finder application is used to measure the height and azimuth of the sun's position at a particular time. Firstly, a coordinate point is selected as the surface location to calculate the zenith angle, the angle of incidence of sunlight, and the declination angle. The declination angle is formed by the equatorial field and the connecting line between the center of the sun and the earth using the Cooper equation directly [26, 27].

$$\delta = 23,45^{\circ} \times sin\left[360\frac{284+n}{365}\right] \tag{1}$$

where, n is the year's day, with January 1 as n = 1, in the Gregorian calendar, each year consists of 365 days, except for one year divisible by four, considered a rough year with 366 days [28].

Secondly is the measurement of the elevation angle (α). The elevation angle is the angle between the horizontal and the line to the sun, which is the complement of the zenith angle (θz), measuring the latitude angle (φ) and declination (δ). In addition, the elevation parameter angle becomes more accurate by considering the change in the elevation angle throughout the day as the sun hour angle (ω) so that the elevation angle can be calculated.

$$\alpha = sin^{-1}[(sin\varphi \times sin\delta) + (cos\varphi\, cos\delta\, cos\omega)] \tag{2}$$

Then, the third step is measuring the azimuth angle (ψ). The azimuth angle is the shift in the angle of the south pole. The projection of solar radiation exposure to the horizontal plane on other conditions also allows for a shift in the angle from the north so that at noon, the angle is 0° from the south and 180° to the north. The azimuth angle can be obtained from the equation:

$$\psi = \sin(\omega)\left|cos^{-1}\left(\frac{cos\theta_z\, sin\emptyset - sin\delta}{sin\theta_z\, cos\emptyset}\right)\right| \tag{3}$$

Figure 6 shows the geometric relationship of several angles as a form of the sun's orbital motion at any time. The shadow ratio (SR%) at each geographic coordinate point can be assumed to be exactly along a straight line parallel to the azimuth angle at any time on the horizontal plane of the surface, and as a second step, the projection of the presence of sunlight, the equation:

$$SR(\%) = \frac{1}{tan\alpha_s} \tag{4}$$

Lastly, a simple linear regression method is used to create a relationship between the coordinate point variables and the azimuth angle gradient as the slope of a straight line.

$$y - y_1 = m\,(x - x_1) \tag{5}$$

where:
- y_1 = Latitude angle;
- x_1 = Longitude angle; and
- m = Azimuth angle

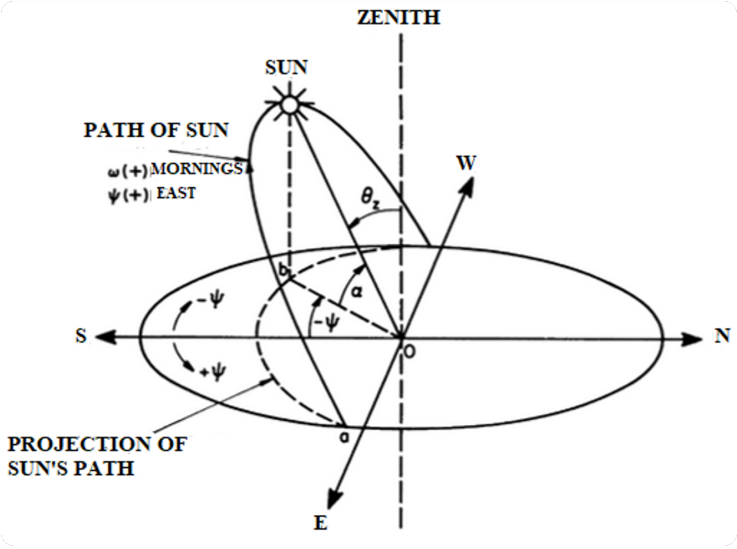

Figure 6. Zenith angle (θz), elevation angle (α), azimuth angle (ψ) as angles forming the position of the sun in the sky

Meanwhile, the distance between geographic coordinate points in the shadow can be calculated through Eq. (6):

$$L_{\text{so}} = 3963 \times cos^{-1}\left(\{(siny_2) \times (siny_1)\} + \{(cosy_1) \times (cosy_2) \times (cos\,(x_2 - x_1)\}\right) \times 1.60 \tag{6}$$

A group of coordinates of points targeted at the peak shadow of the shade profile at each subsequent time change (azimuth). That can be expressed as a shadow projection pattern due to the obstruction of sunlight exposure both at sunrise and sunset in the evening.

2.4.2 Analysis of solar radiation intensity

Studies on solar radiation profiles in Indonesia have been conducted several times, primarily to support the analysis of solar energy potential in Indonesia. Solar energy potential is usually calculated using empirical equations with input from other meteorological parameters, where the most commonly used parameter is the duration of sunlight [28, 29]. An effective and efficient way to meet the availability of adequate radiation data is to create a prediction model based on existing data from various Meteorology, Climatology, and Geophysics Agency or MCGA stations (BMKG stations in Indonesia) or using mathematical equations. Schuepp has developed mathematical equations using solar radiation data outside the atmosphere or standard atmospheric conditions. In contrast, using long exposure data, Angstrom has developed a correlation to predict global solar radiation on the horizontal plane [30]. The advantage of the Angstrom correlation is that it can determine global radiation even though the data is unavailable at the BMKG station. The Angstrom correlation equation is obtained as follows:

$$R_s = \left(a_s + b_s \frac{n}{N}\right) R_a \tag{7}$$

where;
- R_s = Global solar radiation or shortwave (MJ/m^2.day)
- n = Actual sunshine duration (hours)
- N = Maximum sunshine duration or day (hours)
- n/N = Relative sunshine duration
- R_a = Space radiation (extraterrestrial) (MJ/m^2.day)

- a_s = Regression constant, which expresses the fraction of space radiation reaching the earth on cloudy days (n = 0)
- b_s = Fraction of space radiation reaching the earth on clear days (n = N)

R_s will vary depending on atmospheric conditions (humidity, dust), solar declination, and latitude. The Angstrom values a_s and b_s will also vary. If no actual solar radiation data is available and no calibration is done to correct the parameters a_s and b_s, then the recommended values a_s = 0.25 and b_s = 0.50.D [31].

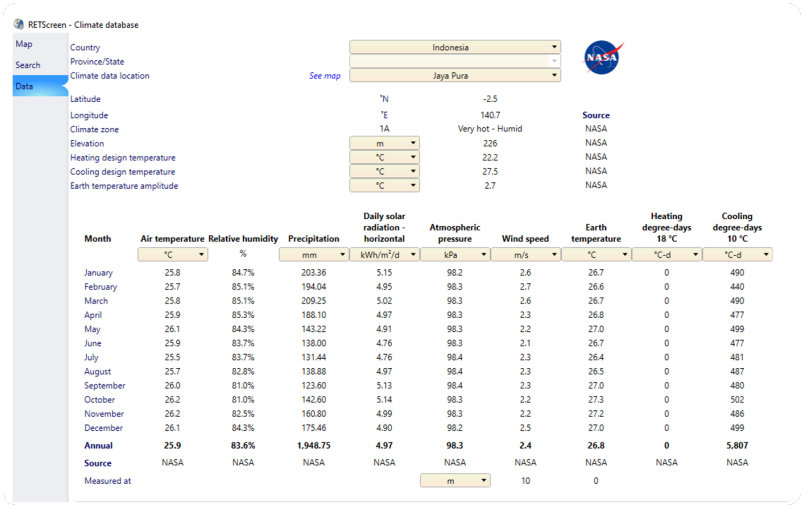

Figure 7. Climate data with the RETScreen application

Table 1. Results of measuring the position of the sun on March 20, 2022 (n= 79)

No.	Time	Elevation (deg)	Azimuth (deg)	RB (%)	No.	Time	Elevation (deg)	Azimuth (deg)	RB (%)
1	06.00	3.8	90.1	14.99	15	12.30	78.4	281.8	0.2
2	06.30	11.3	89.8	5.0	16	13.00	71.0	277.0	0.34
3	07.00	18.8	89.4	2.94	17	13.30	63.6	274.8	0.5
4	07.30	26.3	89.0	2.02	18	14.00	56.1	273.6	0.67
5	08.00	33.8	88.6	1.49	19	14.30	48.6	272.2	0.88
6	08.30	41.3	88.1	1.14	20	15.00	41.1	272.1	1.15
7	09.00	48.8	87.4	0.88	21	15.30	33.6	271.6	2.04
8	09.30	56.2	86.5	0.67	22	16.00	26.1	271.1	2.04
9	10.00	63.7	85.3	0.49	23	16.30	18.6	270.7	2.96
10	10.30	71.2	83.1	0.34	24	17.00	11.1	270.4	5.07
11	11.00	78.6	78.2	0.2	25	17.30	3.7	270.1	15.65
12	11.30	85.6	57.1	0.08	26	18.00	-3.8	269.7	-
13	12.00	85.5	302.0	0.08	27	18.30			

In this paper, solar intensity data obtained from NASA data is used by RETScreen software. RETScreen software provides real-time data such as air temperature, humidity, solar radiation intensity, earth temperature, and atmospheric pressure, as shown in the layer captured in Figure 7.

3 Results

3.1 Analysis of Elevation Angle and Azimuth Position Data

Based on the results of GPS measurements, one of the surface coordinate points in the residential area was selected as a shelter point at Latitude $2°36'10''$SL (-2.6028SL) and $140°39'21''$ EL (140.6558 EL). Secondary data from March 20 and September 23, 2022, obtained from the SLP application, are presented in Table 1 to Table 3. In Table 1 and Table 2, measurements started at $06.00\text{AM} - 18.00\text{PM}$. Changes in the sun's position provide elevation and azimuth angles and SRs that indicate the rotation of the earth on its axis and the earth's revolution around the sun. N (21). In Table 3, a comparison of the position of the sun throughout the year shows that the position of the earth in the southern hemisphere in July is away from the sun with the lowest elevation ($\pm 30°$) because the

position of the earth's latitude is far from the sun, while in January it is closer to the sun. While in March-April and September-October, the declination angle is towards 0°.

Table 2. Results of measuring the position of the sun on September 23, 2022 (n=266)

No.	Time	Elevation (deg)	Azimuth (deg)	RB (%)	No.	Time	Elevation (deg)	Azimuth (deg)	RB (%)
1	06.00	7.7	89.6	7.36	15	12.30	74.5	279.3	0.28
2	06.30	15.2	89.2	3.67	16	13.00	67.1	276.0	0.42
3	07.00	22.7	88.9	2.39	17	13.30	59.6	274.3	0.59
4	07.30	30.2	88.4	1.72	18	14.00	52.2	273.2	0.78
5	08.00	37.7	87.9	1.29	19	14.30	44.7	272.5	1.01
6	08.30	45.2	87.3	0.99	20	15.00	37.2	271.9	1.32
7	09.00	52.7	86.6	0.76	21	15.30	29.7	271.4	1.75
8	09.30	60.2	85.4	0.57	22	16.00	22.2	271.0	2.45
9	10.00	67.6	83.2	0.41	23	16.30	14.7	270.6	3.81
10	10.30	75.0	80.2	0.27	24	17.00	7.2	270.2	7.91
11	11.00	82.3	70.4	0.13	25	17.30	-0,3	269.9	-
12	11.30	87.4	354.1	0.05	26	18.00	-7.8	269.5	-
13	12.00	81.8	288.2	0.14	27	18.30			

3.2 Sun Path Shade Projection

Table 3. Results of measuring the position of the sun every 08.00 in 2022

No.	Date	Day (n)	Elevation(deg)	Azimuth (deg)	SR (%)
1	5 January	5	32.7	115.4	1.55
2	11 February	50	31.9	105.0	1.60
3	21 March	80	33.8	88.1	1.49
4	15 April	105	34.6	76.4	1.45
5	20 May	140	33.1	64.1	1.53
6	19 June	170	30.9	60.6	1.67
7	14 July	195	30.3	62.9	1.71
8	18 August	230	33.0	72.4	1.54
9	17 September	260	36.9	85.1	1.33
10	22 Oktober	295	39.3	102.0	1.22
11	21 November	325	37.7	113.2	1.29
12	31 December	365	34.1	116.7	1.48

Table 4. Results of the analysis of the shadow projection equation on geographic coordinates

No.	Time	SR (%)	Azimuth-m (deg)	Description
1	06.00	14.99	90.1	y=1.571x-3.902
2	06.30	5.00	89.1	y=1.554x-3.589
3	07.00	2.94	89.4	y=1.560x-3.872
4	07.30	2.02	89.0	y=1.553x-3.855
5	08.00	1.49	88.6	y=1.546x-3.838
6	08.30	1.14	41.3	y=1.537x-3.816
7	15.00	1.15	272.1	y=4.747x-11.692
8	15.30	2.04	271.6	y=4.738x-11.671
9	16.00	2.04	271.1	y=4.729x-11.469
10	16.30	2.96	270.7	y=4.722x-11.632
11	17.00	5.07	270.4	y=4.717x-11.619
12	17.30	15.65	270.1	y=4.712x-11.606

Figure 8 and Figure 9 are obtained from the results of Table 1 and Table 2, which show the graph of the relationship between the geometry of the sun's path daily. The highest elevation angle occurs at 12:00 am, which shows that the sun's position is almost directly above the equator in March and September, so the SR is almost directly above the object (0.08%). The azimuth angle towards noon experiences an extreme angle jump because the azimuth angle analysis refers to the north (noon $= 180°$), according to Duffie and Beckman's description [32]. Furthermore, based on the case of Figure 10, the observation applies to rotation and revolution. The movement of the earth towards the sun every hour is the same, so the height of the sun's position with the coordinates of objects on the earth's surface does not experience much difference every day, as well as the comparison of the shadows remains the same but will be very different. There is a change in hours every time due to the earth's rotation.

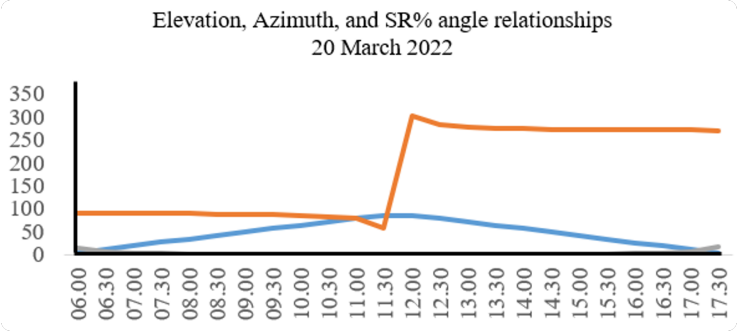

Figure 8. Graph of the geometric relationship of the sun's path (March 20, 2022)

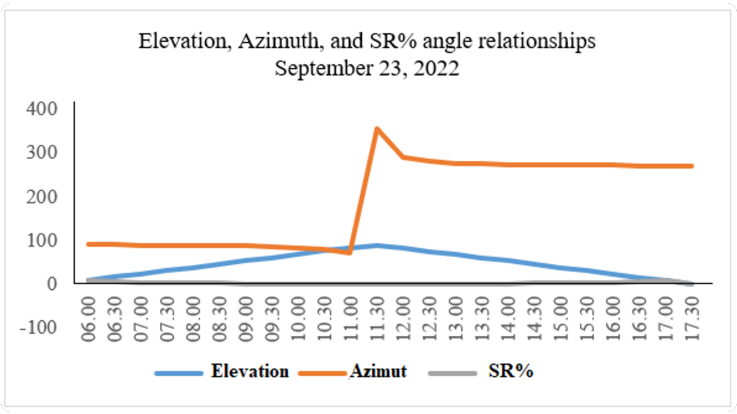

Figure 9. Geometry relationship graph of the sun's path (September 23, 2022)

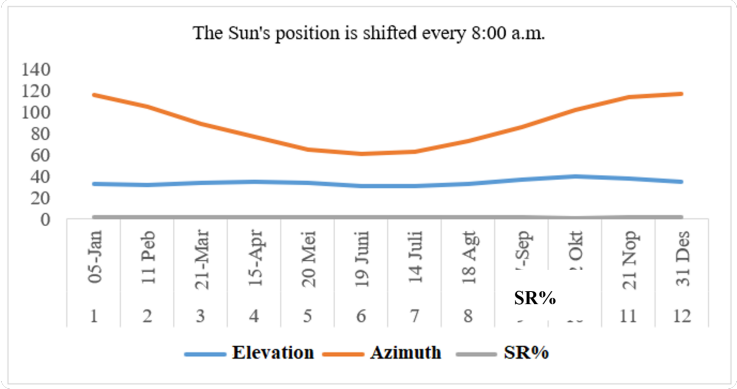

Figure 10. Comparison of changes in geographical angles each month during the Earth's revolution around the sun

To calculate the shadow projection based on the azimuth angle (the angle of inclination of the straight line on the projection of the incoming ray = m) and the geographic coordinate point from Table 1 by applying a simple regression equation, a pair of coordinate points based on the coordinate points that have been determined the results.

From the calculation results, a linear equation determines the shadow projection in Table 4. The equation provides initial information about the potential for shadows along the line formed by a surface coordinate point. The sampling limit is based on the percentage of the shadow ratio (%SR). If the SR is less than one, then the potential shade is relatively small because the sun's position is approaching noon.

3.3 Sun Path Map

Figure 11 shows the results of the analysis of the RETScreen application regarding the map of changes in the position of the elevation angle against changes in the azimuth angle at any time measured every month at the study location, namely, Organda housing. This map provides data conformity by measuring the relationship between the elevation angle, the azimuth angle, and the shadow length ratio, as measured in Table 1, Table 2, and Table 3. In the April to August month cycle, it can be seen that in May, July, and June, the northern hemisphere tends to approach the sun so that the azimuth angle is in the range ($> -90°$ and $< 90°$) with a declination angle of $0° - 23.45°$N. Furthermore, in the January to November month cycle, it can be seen that in February, October, and December, the southern hemisphere approaches the sun so that the azimuth angle is ($< -90°$ and $> 90°$) with a declination angle of $0° - 23.45°$S. Meanwhile, in March-September the azimuth angle is at $(-90° < \psi < 90°)$; this means that in those months, the sun's path almost coincides with the earth's equator with a declination angle of $0°$. In addition, when compared with Table 1, Table 2, and Table 3, the azimuth angle tends to approach $0°$ when the time shows noon (11:00-11:30 am) with a more significant elevation angle (towards $90°$), causing the SR not to exceed the length of the shadow object $< 1\%$). As the afternoon approaches, the azimuth angle value shifts due to changes in the arrival of sunlight from the west. The azimuth angle moves to the east with a value greater than $90°$ and gradually decreases towards sunset.

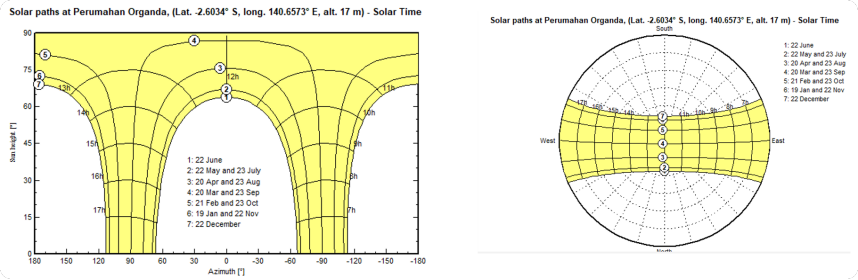

Figure 11. Solar power line in Organda Jayapura housing

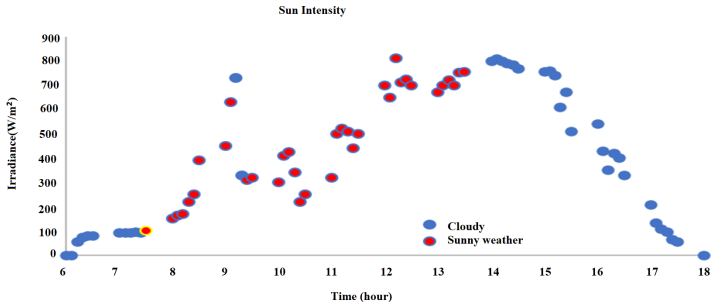

Figure 12. Solar irradiance measurement in December 2022 (MH-1)

3.4 Measurement of Solar Intensity

Based on the reference for measuring the position of the sun, the beginning of the rainy season (MH-1) occurs in December, while the end of the rainy season is in March (MH-2). Furthermore, the beginning of the dry season is in June (MK-1), and the end of the dry season is in September (MK-2). Therefore, it has also been carried out in these months to align the solar radiation intensity measurement data. Alignment of sunny, cloudy, and overcast weather measurements carried out by following the following conditions:

1) Sunny weather refers to the condition of the sky, free from clouds or only a few, so sunlight can shine brightly and the air temperature feels warm. That usually happens in the dry season.

2) Cloudy weather is a condition where the sky is covered by dark clouds that cover most or all of the sky so that sunlight cannot penetrate the clouds properly, and the air temperature feels rather cold, as a sign that rain will fall.

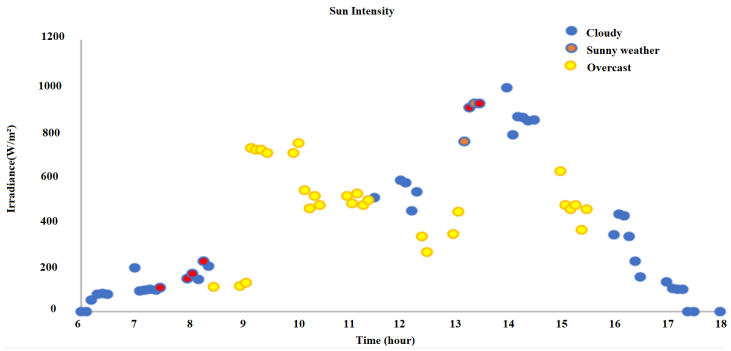

Figure 13. Solar irradiance measurements in March 2023 (MH-2)

3) Cloudy weather is where clouds cover the sky but are not as dense or dark as overcast weather. Clouds can vary in type and thickness, and air temperature varies depending on the type of cloud and the time of day. Cloudy weather usually occurs before or after rain, but it does not always mean rain will fall.

Figure 12, Figure 13, Figure 14, and Figure 15 show the measurements of solar intensity for four seasonal conditions, respectively. Figure 12 shows the initial conditions of the rainy season (MH-1) in December 2022. In this measurement, it can be seen that the solar intensity started at 7:50 am in sunny conditions (red mark) with an irradiation of 102.1 ($\mathrm{W/m^2}$) and continued to increase until 1:50 pm with the highest irradiation of 755 ($\mathrm{W/m^2}$). Although the conditions were cloudy (blue mark) after that, the solar intensity increased to 810 ($\mathrm{W/m^2}$) until 2:10 pm and then decreased until 6:00 pm. This is different from the conditions at the end of the rainy season in March 2023 (MH-2), as shown in Figure 13. Remarkably, a few sunny conditions lasted briefly both in the morning and during the day, between 1-2 hours only, and the rest were dominated by cloudy conditions (blue mark) and overcast (yellow mark).

In the early conditions of the dry season (MK-1) in June 2023, as shown in Figure 14, it can be seen that the sunny, cloudy, and overcast conditions vary. Generally, sunny conditions occur in the morning, starting at 9:40 am with a solar intensity of 475 $\left(\mathrm{W/m^2}\right)$, until noon at 1:50 pm with the highest intensity of 920 $\left(\mathrm{W/m^2}\right)$. After that, the weather changes to cloudy and overcast conditions. This change also affects the change in intensity, which begins to decrease, unlike the early conditions of the rainy season, which experienced an increase in intensity for 2 hours until it decreased until the evening. Next, Figure 15 shows the conditions at the end of the dry season (MK-2) in September 2023. These conditions are almost the same as those at the beginning of the dry season. Changes in sunny, cloudy, and overcast conditions also vary. The sunny conditions that occurred started at 7:50 am with a solar intensity of 99 ($\left(\mathrm{W/m^2}\right)$) and experienced an increase in the highest intensity of 810 $\left(\mathrm{W/m^2}\right)$ at 12:20 am and decreased to 755 $\left(\mathrm{W/m^2}\right)$ at 1:50 pm. Furthermore, there were changes in cloudy and overcast conditions until the evening. In addition, the solar intensity that occurred at the end of the dry season was slightly lower at 810 $\left(\mathrm{W/m^2}\right)$ compared to at the beginning of the dry season at 920 $\left(\mathrm{W/m^2}\right)$.

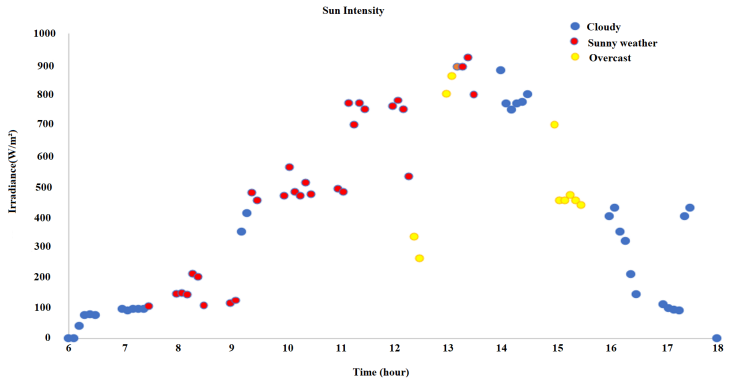

Figure 14. Solar irradiance measurement in June 2023 (MK-1)

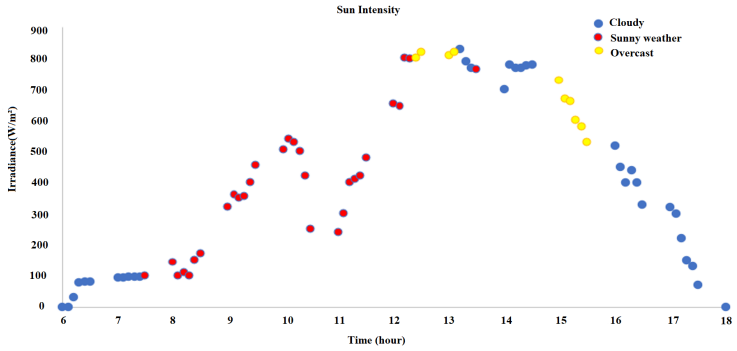

Figure 15. Solar irradiance measurements in September 2023 (MK-2)

3.5 Shadow Ratio (SR)

Shadow areas can occur due to the presence of objects that have a height on the earth's surface that can block direct sunlight so that shadow shade appears. The results of SR measurements at the research site, carried out at any time within a period according to four season categories using the Sun locator software, are shown in Table 5. Changes in the clock time cause the SR value to decrease towards noon, so the SR is quite large when the sun rises and sets. As can be seen, the SR of each research site is the same in the same season category. However, the hourly changes tend to have minimal differences in the SR at each change in the season category. The highest SR occurs at sunrise at 06.00 am and sunset at 06.00 pm. Only the SR of the MH-1 and MH-2 categories can still be measured, while the SR values of MK-1 and MK-2 are no longer visible because the sun has set ($-0°$). The SR is a multiplier factor for the shadow range that causes shade. A site will have the opportunity to be shadowed at a particular hour if the projection of the shadow source has a higher surface peak height than the distance between the site and the shadow source so that the shadow range from the shadow source can shade the site for a while before noon or in the afternoon.

Table 5. Results of SR measurements in 4 different season conditions

Season	Time (Hour)											
	6	7	8	9	10	11	12	13	14	15	16	17
	Shadow Ratio (SR)											
MH-1	8.43	2.67	1.48	0.93	0.6	0.41	0.43	0.56	0.86	0.93	0.60	0.41
MH-2	14.50	2.92	2.92	1.49	0.87	0.49	0.20	0.09	0.68	1.15	2.06	5.17
MK-1	15.08	3.19	1.68	1.06	0.71	0.53	0.50	0.64	0.93	1.45	2.54	7.22
MK-2	7.80	2.44	1.32	0.78	0.42	0.15	0.14	0.42	0.77	1.30	2.41	7.54

4 Discussion

Solar radiation is emitted through electromagnetic waves until it reaches the Earth's surface, so its intensity fluctuations form climate patterns on various time scales [29]. Radiation patterns also provide information in various sectors, including the energy sector. However, solar radiation has yet to be widely studied in various climate studies in Indonesia, considering the lack of solar radiation observation networks and the impact of topographic conditions. Permanent shade is available in specific areas at every earth rotation. The sun's radiation and spatial relationship with the Earth result in an almost constant intensity of solar radiation outside the Earth's atmosphere. The solar constant Gsc is the solar energy per unit time received on a unit surface area perpendicular to the direction of radiation propagation at an average distance between the Earth and the sun outside the atmosphere. Abbott [23] successfully reported the results of their measurements. The solar constant adopted by the World Radiation Center (WRC) is 1367 $\mathrm{W/m^2}$) in sunny conditions. However, only a portion of this value reaches the Earth's surface because several processes occur when entering the Earth's atmosphere, where some of the radiation is mixed and absorbed by particles in the atmosphere [24]. The amount of shortwave radiation that reaches the Earth's surface (horizontal) is called horizontal global radiation, which consists of two types of components: direct and diffuse radiation. As it passes through the atmosphere, solar radiation is partially absorbed, scattered, and reflected by molecules, aerosols, water vapour, and clouds. Direct sunlight that reaches the Earth's surface is called direct solar radiation. Global solar radiation is the total amount of solar radiation that falls on a horizontal surface (i.e., direct sunlight plus solar

radiation scattered on a horizontal surface). Direct solar radiation is observed from sunrise to sunset, while global solar radiation is observed at dusk, before sunrise and after sunset, although its intensity decreases at these times [1].

According to the study by Iqbal [33], direct observations indicate that the solar constant is not truly constant, but rather exhibits variations over days, months, and even years, with potential fluctuations spanning decades. In this paper, variations in the solar constant occur due to changes in the form of solar activity, such as sunspots or bright faculae on the sun's surface. This paper also obtained the same thing; it proved that the Earth's northern hemisphere tends to approach the sun in May, June, and July. In February, October, and December, the Earth's southern hemisphere approaches the sun. Then, according to the research by Raja [34], latitude controls the duration of daylight and the path of oblique rays as the sun sets. Areas with high latitudes usually have lower levels of sunlight, and low latitudes have higher levels. In addition, the climate conditions of the Earth's weather are determined by the interaction of incoming solar radiation with the atmosphere, surface, and ocean. Radiation balance, or net radiation above the top of the Earth's atmosphere, which is the result of radiative exchange between incoming solar radiation and outgoing thermal radiation emitted by the Earth into space, dramatically determines the climate conditions of the Earth. Furthermore, the research by Hoyt et al. [35] suggest that total solar irradiation (solar constant) will decrease with increasing sunspot area and increase with the presence of bright faculae areas on the solar disk.

This study has revealed that Jayapura City has relatively short sunny weather, from around 7:00 am to 1:00 pm, or only 6 hours, even in certain seasons. The rest, cloudy and overcast conditions, are more dominant, so solar power plants can reduce the absorption of solar energy when built in the study area. In sunny conditions, solar cells can absorb sunlight throughout the day. However, the highest absorption efficiency usually occurs between 9:00 am and 3:00 pm. The sun is higher in the sky during this time, so the light intensity is more robust. This means that the opportunity to get adequate solar energy for the needs of PLTS construction in Jayapura City is only 4:00 hours. On the other hand, according to the study by Haider et al. [36], solar energy absorption can be optimised using a tracker. In addition, using a tracker on PLTS can obtain solar energy absorption until 5:00 pm.

Furthermore, sunlight intensity measures the strength of light falling on a surface at a particular time. The higher the light intensity, the more energy can be absorbed by the solar cell. However, it does not mean that the higher the intensity, the better the solar cell's performance [37]. There is an optimal limit at which solar cells can work most efficiently. As is well known, solar cells convert light into electrical energy through the PV effect. When photons (light particles) hit the solar cell, the electrons will be excited and produce an electric current. In addition to light intensity, several other factors also affect the efficiency of solar cell energy absorption, including the type of solar cell, temperature, angle of light impact, and light quality. Monocrystalline, polycrystalline, or thin-film solar cells have different characteristics when absorbing light [38]. Then, the performance of solar cells generally decreases with increasing temperature, and the angle at which sunlight hits the surface of the solar cells also affects efficiency. In addition, the wavelength of light also has an effect, so the design of the solar cell significantly affects the absorption of light in a specific spectrum.

Therefore, several strategies have been proposed to optimise the absorption of solar energy by PV cells, including the selection of locations based on altitude, orientation, and slope [39]. In general, higher elevations tend to experience greater light intensity due to reduced atmospheric obstruction, and solar panels should be oriented optimally towards the sun, typically to the south in the northern hemisphere. Then, the tilt of the solar panels also needs to be adjusted to the geographical latitude to maximize exposure to sunlight throughout the year. According to the research by Afif and Martin [40], the right location is to avoid areas that can block direct sunlight exposure because the efficiency of solar panels can decrease due to shade. The causes are passing clouds, tall buildings, trees, dust, bird droppings, and even between the sides of the panel. For this reason, ideally, it should be on flat land or avoid sources of obstruction such as mountain peaks. However, serious problems can arise if the solar panel site is on the east or west side with a fairly steep slope from a surface peak or if the solar panel installation area is in a valley due to significant topographic differences that affect the potential for receiving solar radiation.

Another strategy is tracking systems, reflectors, and cooling and cleaning solar panels. Solar panels can move following the sun's movement throughout the day on one axis (horizontal or vertical) to allow for more precise position adjustments. Then, the reflectors can reflect sunlight on the solar panels, especially when the light intensity is low or when there are obstacles. According to the study by Saleem et al. [41], generally, the phenomenon that occurs when shade falls on a solar module is the same, which causes the current or voltage of the solar module to decrease according to the type of shade. There are two types of shade, namely soft shade and hard shade. When a soft shade covers the solar module, the current decreases, which causes the module power to decrease, while in the case of a hard shade, the voltage drops drastically, and the power decreases. In addition, a cooling system can help keep the temperature of the solar cells low, thereby increasing efficiency, and cleaning the solar panels from dust, dirt, or snow that sticks to the solar panels can reduce the amount of light reaching the solar cells.

5 Conclusions

This study has succeeded in developing a practical methodology for predicting and assessing the projection of solar radiation intensity shading in Jayapura City. The resulting shading projection map can be a handy tool in planning and developing PLTS in this city. The results of this prediction can be used as a basis for more optimal planning in the utilization of solar energy, such as determining the appropriate solar panel capacity and designing an efficient solar energy system. According to statistics from the State Electricity Company (in Indonesia: PLN), using solar energy through PLTS or solar cells in 2021, Papua Province contributed a capacity of 2.6 MW (12% of the national scale). However, compared to the capacity of power requirements in the Papua Province from fossil fuel energy sources (106.78 MW), the difference is still huge (95.24%).

To address climate change and strengthen the energy supply in Jayapura city, the deployment of renewable energy must be accelerated. This is to the targets of the Indonesian Government for 2025 to 2030 and 2050, namely increasing the use of renewable energy by 23%, 31%, and 50%, respectively, by reducing the use of coal and petroleum. Future work and solar energy exploration can improve by building a PLTS in Jayapura with the correct position. Several alternatives for optimising PLTS have been predicted but have been limited by the sun's path movement pattern and shade.

Author Contributions

Conceptualization, U.T.; methodology, U.T.; software, S.S.; validation, G.C., M. and A.W.H.; formal analysis, U.T.; investigation, S.S.; resources, U.T.; data curation, G.C.; writing—original draft preparation, S.S.; writing—review and editing, G.C.; visualization, M.; supervision, G.C.; project administration, A.W.H.; funding acquisition, U.T.

Data Availability

The data used to support the findings of this study are available from the corresponding author upon request.

Conflicts of Interest

The authors declare no conflict of interest.

References

[1] H. H. Pourasl, R. V. Barenji, and V. M. Khojastehnezhad, "Solar energy status in the world: A comprehensive review," *Energy Rep.*, vol. 10, pp. 3474–3493, 2023. https://doi.org/10.1016/j.egyr.2023.10.022

[2] A. O. Maka and J. M. Alabid, "Solar energy technology and its roles in sustainable development," *Clean Energy*, vol. 6, no. 3, pp. 476–483, 2022. https://doi.org/10.1093/ce/zkac023

[3] D. S. Permana, "Analisis data meteorologi dari pemantau cuaca otomatis berbagai elevasi dan data radiosonde di Papua," *J. Meteorol. dan Geofis.*, vol. 12, no. 2, 2011. https://doi.org/10.31172/jmg.v12i2.96

[4] Sutiyo, "Jayapura municipality in figures 2021," 2021. https://jayapurakota.bps.go.id/publication/2021/02/26/97fbc97aaac3a20d63353a75/kota-jayapura-dalam-angka-2021.html

[5] P. Harahap, I. Nofri, and S. Lubis, "PLTS 200 Wp to meet energy needs at the Taqwa Muhammadiyah Mosque, Sei Litur Village, Sawit Sebrang Langkat District," *J. Innov. Community Engagem.*, vol. 1, no. 1, pp. 60–71, 2021. https://doi.org/10.28932/jice.v1i1.3380

[6] S. K. A. Sudirman Syam, Z. Arifin, and U. Tahir, "Planning and development of solar cells for illumination of dragon fruit and fish pools at the farming group of Kampung Daun, Baumata-Kupang," *Int. Res. J. Adv. Eng. Sci.*, vol. 7, no. 4, pp. 140–145, 2022. http://irjaes.com/wp-content/uploads/2022/11/IRJAES-V7N4P138Y22.pdf

[7] A. Tsikalakis, T. Tomtsi, N. D. Hatziargyriou, A. Poullikkas *et al.*, "Review of best practices of solar electricity resources applications in selected Middle East and North Africa (MENA) countries," *Renew. Sustain. Energy Rev.*, vol. 15, no. 6, pp. 2838–2849, 2011. https://doi.org/10.1016/j.rser.2011.03.005

[8] A. Comber, M. Umezaki, R. Zhou, Y. Ding, Y. Li, H. Fu, H. Jiang, and A. Tewkesbury, "Using shadows in high-resolution imagery to determine building height," *Remote Sens. Lett.*, vol. 3, no. 7, pp. 551–556, 2012. https://doi.org/10.1080/01431161.2011.635161

[9] W. Zhai, W. Zhang, B. Chen, and C. Cheng, "Hyperspectral analysis of objects under shadow conditions based on field reflectance measurements," *Appl. Opt.*, vol. 58, no. 17, 2019. https://doi.org/10.1364/AO.58.004797

[10] F. M. Zaihidee, S. Mekhilef, M. Seyedmahmoudian, and B. Horan, "Dust as an unalterable deteriorative factor affecting PV panel's efficiency: Why and how," *Renew. Sustain. Energy Rev.*, vol. 65, pp. 1267–1278, 2016. https://doi.org/10.1016/j.rser.2016.06.068

[11] X. P. Zhao, P. P. Guo, Z. L. Zhang, X. C. Wang, H. X. Peng, and M. K. Wang, "Wood density and fiber dimensions of root, stem, and branch wood of Populus ussuriensis Kom. trees." *BioRes.*, vol. 13, no. 3, pp. 7026–7036, 2018. https://doi.org/10.15376/biores.13.3.7026-7036

[12] Z. H. Wang, Y. Li, K. Wang, and Z. M. Huang, "Environment-adjusted operational performance evaluation of solar photovoltaic power plants: A three stage efficiency analysis," *Renew. Sustain. Energy Rev.*, vol. 76, pp. 1153–1162, 2017. https://doi.org/10.1016/j.rser.2017.03.119

[13] S. A. Said, G. Hassan, H. M. Walwil, and N. Al-Aqeeli, "The effect of environmental factors and dust accumulation on photovoltaic modules and dust-accumulation mitigation strategies," *Renew. Sustain. Energy Rev.*, vol. 82, pp. 743–760, 2018. https://doi.org/10.1016/j.rser.2017.09.042

[14] A. A. Babatunde, S. Abbasoglu, and M. Senol, "Analysis of the impact of dust, tilt angle and orientation on performance of PV plants," *Renew. Sustain. Energy Rev.*, vol. 90, pp. 1017–1026, 2018. https://doi.org/10.1016/j.rser.2018.03.102

[15] M. R. Maghami, H. Hizam, C. Gomes, M. A. Radzi, M. I. Rezadad, and S. Hajighorbani, "Power loss due to soiling on solar panel: A review," *Renew. Sustain. Energy Rev.*, vol. 59, pp. 1307–1316, 2016. https://doi.org/10.1016/j.rser.2016.01.044

[16] A. Niewienda and F. D. Heidt, "SOMBRERO: A PC-tool to calculate shadows on arbitrarily oriented surfaces," *Sol. Energy*, vol. 58, no. 4-6, pp. 253–263, 1996. https://doi.org/10.1016/S0038-092X(96)00088-6

[17] E. Shaviv and A. Yezioro, "Analyzing mutual shading among buildings," *Sol. Energy*, vol. 59, no. 1-3, pp. 83–88, 1997. https://doi.org/10.1016/S0038-092X(96)00103-X

[18] K. Sinapis, C. Tzikas, G. Litjens, M. Van den Donker, W. Folkerts, W. Van Sark, and A. Smets, "A comprehensive study on partial shading response of c-Si modules and yield modeling of string inverter and module level power electronics," *Sol. Energy*, vol. 135, pp. 731–741, 2016. https://doi.org/10.1016/j.solener.2016.06.050

[19] E. G. Melo, M. P. Almeida, R. Zilles, and J. A. B. Grimoni, "Using a shading matrix to estimate the shading factor and the irradiation in a three-dimensional model of a receiving surface in an urban environment," *Sol. Energy*, vol. 92, pp. 15–25, 2013. https://doi.org/10.1016/j.solener.2013.02.015

[20] M. R. Assadi, M. Ataebi, E. sadat Ataebi, and A. Hasani, "Prioritization of renewable energy resources based on sustainable management approach using simultaneous evaluation of criteria and alternatives: A case study on Iran's electricity industry," *Renew. Energy*, vol. 181, pp. 820–832, 2022. https://doi.org/10.1016/j.renene.2021.09.065

[21] M. F. Lee, S. J. Lim, P. W. Siew, and B. T. Tee, "Technical and economic analysis of solar energy powered lighting system in a smart building at tropical region," in *2022 IEEE International Conference on Industrial Engineering and Engineering Management (IEEM)*, *Kuala Lumpur, Malaysia*, 2022, pp. 407–411. https://doi.org/10.1109/IEEM55944.2022.9989620

[22] Y. T. Yürek, M. Bulut, B. Özyörük, and E. Özcan, "Evaluation of the hybrid renewable energy sources using sustainability index under uncertainty," *Sustain. Energy, Grids Networks*, vol. 28, p. 100527, 2021. https://doi.org/10.1016/j.segan.2021.100527

[23] D. Abbott, "Keeping the energy debate clean: How do we supply the world's energy needs?" *Proc. IEEE*, vol. 98, no. 1, pp. 42–66, 2010. https://doi.org/10.1109/JPROC.2009.2035162

[24] S. R. Pendem and S. Mikkili, "Modeling, simulation and performance analysis of solar PV array configurations (Series, Series–Parallel and Honey-Comb) to extract maximum power under Partial Shading Conditions," *Energy Rep.*, vol. 4, pp. 274–287, 2018. https://doi.org/10.1016/j.egyr.2018.03.003

[25] C. Saiprakash, A. Mohapatra, B. Nayak, and S. R. Ghatak, "Analysis of partial shading effect on energy output of different solar PV array configurations," *Mater. Today Proc.*, vol. 39, pp. 1905–1909, 2021. https://doi.org/10.1016/j.matpr.2020.08.307

[26] Y. El Mghouchi, A. El Bouardi, Z. Choulli, and T. Ajzoul, "Models for obtaining the daily direct, diffuse and global solar radiations," *Renew. Sustain. Energy Rev.*, vol. 56, pp. 87–99, 2016. https://doi.org/10.1016/j.rser.2015.11.044

[27] P. I. Cooper, "The absorption of radiation in solar stills," *Sol. Energy*, vol. 12, no. 3, pp. 333–346, 1969. https://doi.org/10.1016/0038-092X(69)90047-4

[28] L. A. Farah, M. Saifulloh, and J. Roesuldi, "Studi komparasi sejarah dan aturan kalender tahun masehi: Julian dan gregorian," *AL - AFAQ J. Ilmu Falak dan Astron.*, vol. 4, no. 1, pp. 65–77, 2022. https://doi.org/10.20414/afaq.v4i1.4361

[29] G. Kopp, "An assessment of the solar irradiance record for climate studies," *J. Sp. Weather Sp. Clim.*, vol. 4, p. A14, 2014. https://doi.org/10.1051/swsc/2014012

[30] M. Iqbal, *An Introduction to Solar Radiation*. Academic Press, 1983. https://doi.org/10.1016/b978-0-12-373750-2.x5001-0

[31] X. Zhang, J. Wu, H. Wu, H. Chen, and T. Zhang, "Improving temporal extrapolation for daily evapotranspiration using radiation measurements," *J. Appl. Remote Sens.*, vol. 7, no. 1, p. 073538, 2013. https://doi.org/10.1117/1.JRS.7.073538

[32] J. A. Duffie and W. A. Beckman, *Solar Engineering of Thermal Processes*. John Wiley & Sons, Inc., 2013.

https://doi.org/10.1002/9781118671603
[33] M. Iqbal, *Chapter 3 - The solar constant and its spectral distribution*, 1983. https://doi.org/10.1016/B978-0-12-373750-2.50008-2
[34] I. A. Raja, "Insolation-sunshine relation with site elevation and latitude," *Sol. Energy*, vol. 53, no. 1, pp. 53–56, 1994. https://doi.org/10.1016/S0038-092X(94)90605-X
[35] D. V. Hoyt, H. L. Kyle, J. R. Hickey, and R. H. Maschhoff, "The Nimbus 7 solar total irradiance: A new algorithm for its derivation," *J. Geophys. Res. Space Phys.*, vol. 97, no. A1, pp. 51–63, 1992. https://doi.org/10.1029/91JA02488
[36] M. R. Haider, A. Shufian, M. N. Alam, M. I. Hossain, R. Islam, and M. A. Azim, "Design and implementation of three-axis solar tracking system with high efficiency," in *2021 International Conference on Information and Communication Technology for Sustainable Development (ICICT4SD)*, *Dhaka, Bangladesh*, 2021, pp. 1–5. https://doi.org/10.1109/ICICT4SD50815.2021.9396779
[37] V. R. Vadiyala, "Sunlight to sustainability: A comprehensive analysis of solar energy's environmental impact and potential," *Asia Pac. J. Energy Environ.*, vol. 7, no. 2, pp. 103–110, 2020. https://doi.org/10.18034/apjee.v7i2.711
[38] O. Ayadi, R. Shadid, A. Bani-Abdullah, M. Alrbai, M. Abu-Mualla, and N. Balah, "Experimental comparison between Monocrystalline, Polycrystalline, and Thin-film solar systems under sunny climatic conditions," *Energy Rep.*, vol. 8, pp. 218–230, 2022. https://doi.org/10.1016/j.egyr.2022.06.121
[39] M. Zainuddin and H. Annur, "Optimasi penempatan dan kapasitas PLTS on grid pada sistem distribusi radial menggunakan metode algoritma genetika multi konstrain," *J. Rekayasa Elektr.*, vol. 15, no. 1, 2019. https://doi.org/10.17529/jre.v15i1.12507
[40] F. Afif and A. Martin, "Tinjauan potensi dan kebijakan energi surya di Indonesia," *J. Engine Energi, Manufaktur, dan Mater.*, vol. 6, no. 1, pp. 43–52, 2022. https://doi.org/10.30588/jeemm.v6i1.997
[41] A. Saleem, K. Mehmood, and F. Rashid, "The efficiency of solar PV system," in *Proceedings of 2nd International Multi-Disciplinary Conference, Gujrat*, 2019.

Nomenclature

a_s	Regression constant
b_s	Fraction of space radiation reaching the earth on clear days $(\mathrm{n} = \mathrm{N})$
GPS	Global positioning system
$MH-1$	Beginning of the rainy season
$MH-2$	The end of the rainy season
$MK-1$	The beginning of the dry season
$MK-2$	The end of dry season
$MCGA$	Meteorology, Climatology and Geophysics Agency
N	Actual sunshine duration (hours)
n/N	Relative sunshine duration
PV	Photovoltaic
R_a	Space radiation ($\mathrm{MJ/m^2}$.day)
RI	Republic of Indonesia
R_s	Global solar radiation ($\mathrm{MJ/m^2}$.day)
$SPGS$	Solar power generation system
SLP	Sun locator pro
SR	Shadow ratio
SPM	Solar Power Meter
WRC	World Radiation Center

Greek symbols

α	elevation angle
φ	latutide angle
δ	declination
ω	sun hour angle
ψ	azimuth angle
θz	zenith angle